J Mater Sci (2011) 46:6916–6924
DOI 10.1007/s10853-011-5657-7

The phase stability in Cr–Ni and Cr–Mn duplex stainless steels

I. Calliari · M. Pellizzari · M. Zanellato · E. Ramous

Received: 28 March 2011 / Accepted: 24 May 2011 / Published online: 4 June 2011
© Springer Science+Business Media, LLC 2011

Abstract The formation of secondary phases during isothermal treatments in the range 750–1000 °C and continuous cooling in 2205, 2507, 2304, and 2101 duplex stainless steels have been investigated. For all the steels herein considered, the Thermocalc calculations indicate the sigma and chi-phase precipitation which is confirmed by the experimental results only for the 2205 and 2507 grades. On the contrary, the secondary phases are very rarely observed after both isothermal aging (up to 750 h) and/or continuous cooling tests in the 2304 and 2101 Cr–Mn grades. This behavior could be justified by the different ferrite and austenite phase stability in the four grades, in the same temperature range of the sigma and chi precipitation, because these differences affect the dangerous phases precipitation mechanism and kinetic.

Introduction

The preferred microstructure for the duplex stainless steels (DSS) is a dual-phase microstructure with an almost equal parts of austenite and ferrite [1–3], which give them a favorable combination of mechanical and corrosion properties. This microstructure results from a ferrite to austenite solid phase transformation after the solidification and is obtained by an accurate balance of the chemical composition and by a suitable solution annealing heat treatment, which temperature actually determines the phase proportion [4].

The desired microstructure and technological properties are obtained by adjusting the compositions with addition of well equilibrated amounts of Cr, Mo, Ni, and Mn to the base Fe–Cr alloy. However, such additions affect both the relative stability of austenite and ferrite phases, and can induce the formation of secondary phases in the temperature range below 1000 °C, either during service or during fabrication, and this can be dangerous both for corrosion and the mechanical properties. Therefore, thermomechanical treatments are always necessary, such as a solution annealing followed by rapid quenching from temperature above 1000 °C, both to avoid secondary phase's formation and to maintain the balanced microstructure of ferrite and austenite, stable only at temperatures above 1000 °C. These phenomena are well-known and have been extensively studied, because they condition the behavior of DSS both in service and during fabrication.

Indeed, for a useful exploitation of the DSS a profound knowledge of secondary phase formation is necessary, mainly in two practical situations: during the cooling from high temperatures, as in the quenching treatment after solution annealing or after welding operations, and during long time maintenance at high temperatures, during service, for instance. With this in mind, therefore, a study of the microstructure transformations, occurring in the DSS both by continuous cooling tests (CCT) and by isothermal treatments is required to analyze the possible formation of dangerous phases in the two separate situations.

However, the mechanism and sequence of secondary phase formation seems to be different in DSS of different composition, as in the Cr–Ni (2205 and 2507 grades) and the Cr–Mn (2101 and 2304 grades) DSS. Moreover, the conditions, like time, temperature, cooling rate for

I. Calliari · M. Zanellato · E. Ramous (✉)
DPCI, University of Padova, Padova, Italy
e-mail: emilio.ramous@unipd.it

M. Pellizzari
DMEIT, University of Trento, Trento, Italy

secondary phases formation seems to vary for different DSS grades [5–15].

Therefore, it is interesting to analyze and to compare the sequence of secondary phases formation in some commonly used DSS grades: the results could be useful also to correlate the differences of behavior with the different compositions of the DSS grades examined.

Experimental

The as-received material were wrought SAF 2205, 2507, 2304, and 2101 DSS rods and bars (30 mm).Their chemical compositions are reported in Table 1.

Isothermal aging treatments of specimens, previously solution annealed at 1020 or 1050 °C for 30 min were carried out in the temperature range 650–1000 °C. Both relatively short aging times were chosen (5–120 min), to measure low amounts of secondary phases and investigate their precipitation kinetics, and long times aging (up to about 750 h), to investigate the behavior of low nickel DSS steels.

Continuous cooling tests have been performed in a Setaram "Labsys TG" machine, in Argon atmosphere. Samples (diameter 6 mm, length 8 mm) were heated at 10 °C/min from RT and solution treated (maintenance for 5 min) at temperatures of 1020 and 1050 °C, then cooled in argon at various cooling rates in the range 0.02–0.4 °C/s.

Different phases have been identified by SEM using backscattered electrons (SEM-BSE) examination of unetched samples. The ferrite appears slightly darker than austenite, while the secondary phases are lighter. Owing to the higher content of molybdenum, in combination with the large atomic scattering factor of molybdenum χ-phase appears in brighter contrast than σ-phase [16]. On the contrary, nitrides and carbides appear as black particles, owing to lower atomic scattering factor of nitrogen and carbon. The amount of secondary topologically close-packed (TCP) phases has been determined using image analysis software on SEM-BSE micrographs on polished samples without etching (medium value of examinations on ten fields, 1000×). The chemical composition of the phases was determined by SEM using energy dispersive spectroscopy (EDS), on unetched samples. The volume fractions of ferrite and austenite in solution treated samples have been measured on three longitudinal and three transversal sections (20 fields for each section) by image analysis on light micrographs at 200×, after etching with the Beraha's reagent (RT, 10 s).

In this study, the thermodynamic modeling is based on the CALPHAD method (CALculation of PHAse Diagrams) [17]. The software ThermoCalc [18] was used in connection with the thermodynamic database TCFe3. The method is based on the minimization of Gibbs free energy of the phases provided by the Fe–C–Si–Mn–Cr–Ni–Mo–N multicomponent system. The analytic description of the Gibbs free energy is based on the sublattice model, characterized by atoms arrangement in several sub-lattices. In the case of ferrite and austenite phase in the duplex system, two subgrids are used, one for the metal and one for interstitial atoms. Vacancies are also taken into account, to consider that not all sites are occupied. In the case of other phases, e.g., $M_{23}C_6$ carbides, four subgrids are provided for the metal atoms and one for the interstitials.

Equilibrium data

The microstructures of solution annealed, isothermal aged, and continuous cooled samples can be analyzed and discussed relating them to the equilibrium microstructures which can be derived from Thermocalc calculations and other equilibrium phase diagrams. The results of Thermocalc calculations are shown in Fig. 1: the diagrams, displaying the mole fraction of phases as a function of temperature, present a rather similar general pattern but also some significant differences for all the grades:

1. The solidification produces a ferrite solid phase which gradually and partially transforms to austenite as the temperature decreases; therefore, in all steels at 1020–1080 °C the microstructure consists of almost equivalent parts of austenite and ferrite.
2. At temperatures below 400 °C, the microstructure consists mainly of ferrite, with some minor constituents as χ-phase, other intermetallics and chromium

Table 1 Steels compositions

	C	Si	Mn	Cr	Ni	Mo	Cu	W	P	S	N
2205	0.030	0.56	1.46	22.75	5.04	3.19	–	–	0.025	0.002	0.16
2507	0.030	0.43	0.54	24.48	6.36	4.0	0.67	0.72	0.020	0.008	0.263
2101	0.026	0.69	3.95	22.57	1.1	0.07	–	–	0.03	0.001	0.13
2304	0.03	0.56	1.4	23.20	4.3	0.18	–	–	0.027	0.001	0.10

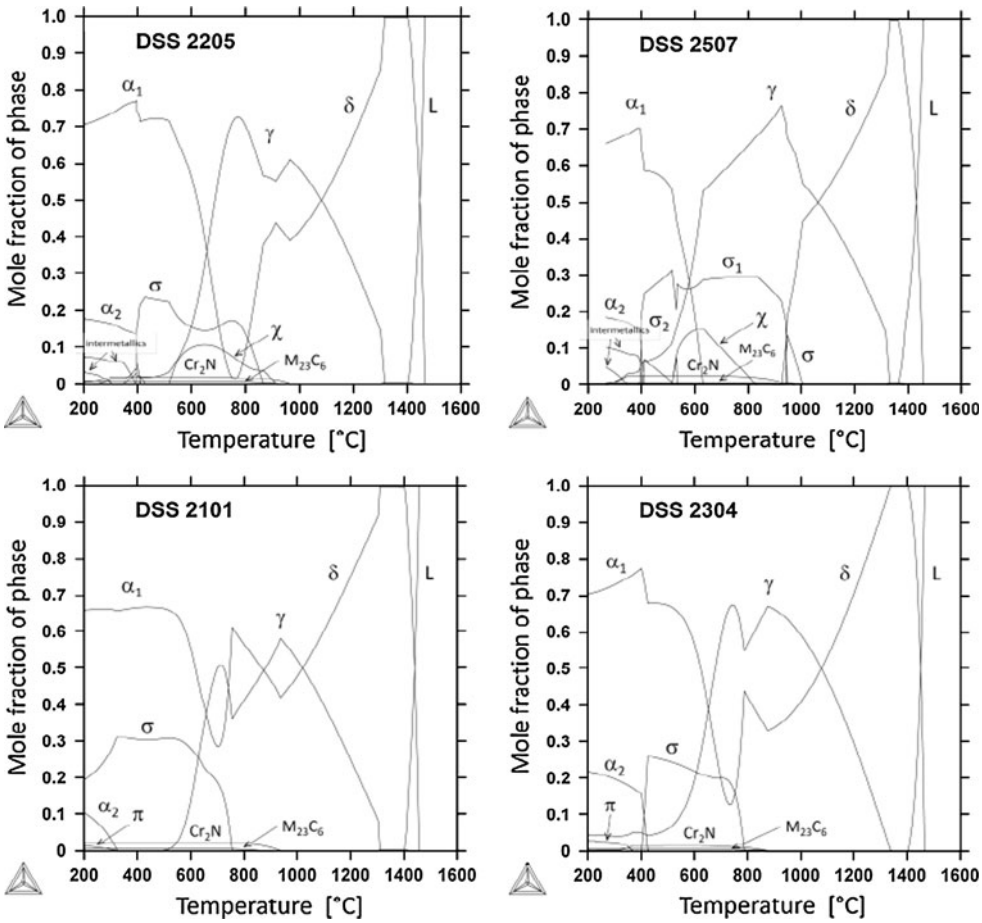

Fig. 1 Thermocalc diagrams of the four DSS

carbides and nitrides; just in one case, i.e., 2101 grade, σ-phase is indicated also below this temperature.

Moreover, the Thermocalc diagrams highlight some significant differences:

3. The maximum temperature of the σ-phase formation decreases for 2507 steel, to 2205, 2304, and 2101 steels, in this order, from about 1000 to about 750 °C.
4. Only in the 2507 and 2205 grades, the σ-phase formation occurs together with the disappearance of the ferrite which transform to σ and secondary austenite and, at very low temperatures, the austenite partially transforms to ferrite, leaving the σ unchanged.
5. On the contrary, in 2101 grade, the σ-phase formation occurs without the complete transformation of ferrite to secondary austenite; at low temperatures, as in 2507 and 2205 grades, austenite transforms to ferrite.
6. The behavior of the 2304 steel appears as intermediate: during the σ formation ferrite partially transform to secondary austenite, therefore, a significant ferrite content remains in all the considered temperature range.
7. The formation of the χ-phase is predicted only for 2205 and 2507, the grades having the highest Mo content, while this is not for the 2101 and 2304 grades.

Results and discussion

Solution annealing

For all the examined steels, the microstructure obtained after solution annealing and quenching was typical of the DSS rolled products, as concerning the ferrite/austenite ratio. The banded structure of elongated austenite islands was observed in the longitudinal sections, while the isotropic structure of ferrite and austenite grains was displayed on the transverse sections. The values of ferrite volume fractions, measured on longitudinal and transverse sections, are about 50–55%, as expected for these steels. The differences between transversal and longitudinal data are less than standard deviations; consequently all the quantifications were performed on the transverse sections. Secondary phases were not detected in the annealed materials before the isothermal aging, in agreement with thermodynamic calculations (Fig. 1).

2205 and 2507 grades

Isothermal aging

In the 2205 grade, the precipitation of secondary phases occurs after aging in the range 780–900 °C (Fig. 2). The precipitation sequence can be summarized as follows:

- 780 °C: The first precipitates appear after 30′ aging and become more evident after 40′. The small bright particles were identified as χ-phase by the SEM–EDS, just within the beam resolution limit.
- 850 °C: The χ-phase appears after about 10′, while the σ-phase after about 20′; after 30′, the χ-phase and the σ-phase are both present: the χ-phase is always at the boundaries austenite/ferrite and ferrite/ferrite. The σ-phase penetrates the ferrite or grows along the austenite/ferrite boundaries
- 900 °C: Also at this temperature the first precipitating phase is the χ-phase, generally decorating the grain boundaries. By increasing the holding time, the amount of χ-phase increases and also the σ-phase appears, as coarse precipitates at the austenite/ferrite boundary, but growing into the ferrite (Fig. 2). Although σ particles are, at the beginning, less numerous than the χ-phase particles, they are coarser, and grow more rapidly, almost reaching the same volume fraction in a short time. He et al. [8] also evidenced the higher growth rate of σ-phase than χ-phase at high temperature. By increasing the holding time, σ-phase grows to large particles, moving from the boundaries into the ferrite, embedding some small χ particles. This seems to show the progressive transformation of χ-phase to σ-phase confirming the experimental evidence that χ-phase provides suitable nucleation sites to σ-phase, in good agreement with other researches [6–8, 19]. From this point of view, the absence of σ at 900 °C in the equilibrium diagram (Fig. 1a) confirms that Thermo-calc underestimates the precipitation temperature of this phase. In view of recent results regarding 2205, calculated by TCFe6 [8], it is believed that this is due to the use of a relative old TCFe3 database.

In the 2507 grade, the precipitation of secondary phases occurs at higher temperatures than in the 2205 grade, i.e., between 850 and 1000 °C [7, 9]. The precipitation sequence is very similar to the 2205 grade, and can be summarized as follows:

- 850 °C: χ-phase is the only one phase to precipitate at the ferrite/austenite boundaries (volume fraction < 0.1%).
- 900 °C: At this temperature, the formation kinetic of χ-phase is favored (Figs. 3, 4).

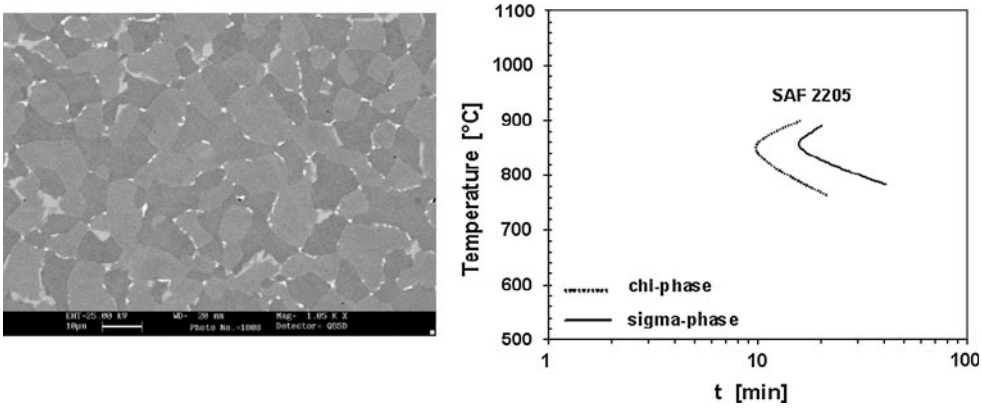

Fig. 2 2205 isothermal aging: *left* SEM-BSE micrograph after 25 min at 900 °C. *right* σ and χ precipitation kinetics

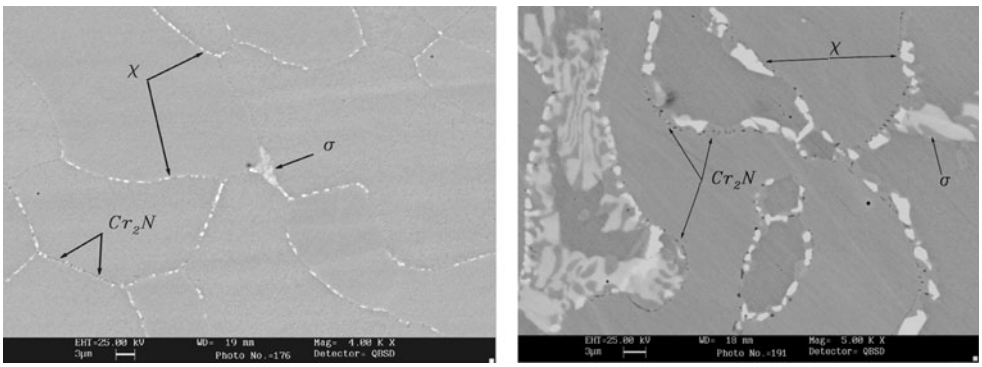

Fig. 3 BSE of 2507. *Left* (900 °C, 5 min) and *right* (950 °C, 40 min) nitrides and chi-phase transforming to sigma-phase

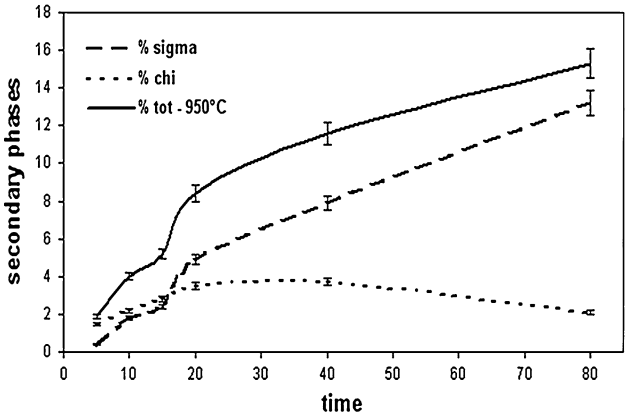

Fig. 4 Volume fractions of secondary phases in 2507 aged at 950 °C

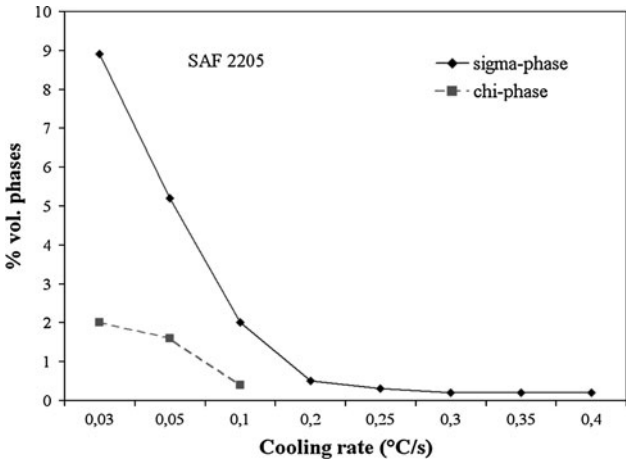

Fig. 5 Sigma and chi (vol.%) versus cooling rate in the 2205 DSS, solution annealed at 1120 °C

– 950 °C: χ-phase is the first to precipitate after 3′, followed by σ after 5′. By increasing aging time, σ grows to large particles, moving from the boundaries into the ferrite, embedding some small χ particles, which seem to behave as preferential sites for the χ-phase nucleation. The trend in Fig. 4 seems to confirm that only σ-phase can be expected under long time exposition, i.e., approaching equilibrium conditions, as suggested by Thermocalc calculations.
– 1000 °C: After 5′, χ and σ-phases are mainly at grain boundaries and a few inside the ferrite grains (about 0.5%). By increasing the time, the content of χ slowly decreases while the amount of σ increases to its maximum value of 4% after 15′.

In all the samples treated at 900–950 °C, small nitrides were detected at grain boundaries.

Looking at the diagram of 2507 steel in Fig. 1, it can be deduced that Thermocalc underestimates the precipitation temperatures of both χ and σ-phases.

Continuous cooling

The morphology and localization of the secondary phases after continuous cooling are very similar to that observed in the isothermal aging tests (the precipitation occurs at the ferrite/austenite grain boundaries and mostly at the triple points), while the formation sequence of secondary phases seems to be different.

In the 2205 grade, the total amount of secondary phases is lower for the highest solution annealing temperature, in agreement with [10], and is strongly dependent both on the cooling rates and on annealing temperature (see Fig. 5). At the highest cooling rates, the secondary phase precipitation is completely avoided. As the cooling rate slows down, the σ-phase appears as the first phase: the critical cooling rate for σ-phase formation is 0.35 °C/s, corresponding to a σ-phase content of 0.2%.

With a further lowering of the cooling rate, the σ-phase content gradually increases and at about 0.1–0.15 °C/s a small amount of χ-phase appears; therefore, the χ-phase appears at lower cooling rates than the σ-phase [8, 10].

The sequence of precipitation during continuous cooling seems to be different from that obtained by isothermal aging. In the latter, the χ-phase is always the first precipitating phase while in the continuous cooling the same sequence occurs only at low cooling rates, and at the highest cooling rate the χ-phase formation seems to be unattainable .

The effects of continuous cooling treatments in the 2507 are very similar to that of the 2205 grade and can be summarized:

– The total amount of secondary phases is slightly lower for the highest solubilization temperature (1120 °C), in agreement with the results obtained for 2205.
– The amount of secondary phases and the relative morphology are quite similar for both the solution temperatures; the secondary phase volume fraction increases if the cooling rate decreases.
– The cooling rate corresponding to the first precipitation, less than 1%, can be estimated to be 0.8–0.9 °C/s.

Secondary phase composition

Further information on the secondary phase precipitation in 2205 and 2507 grades can be derived from the chemical composition of the phases, after the different heat treatments considered.

The compositions of χ-phase and σ-phase in the 2205 steel after isothermal aging (Table 2) and continuous cooling treatments (Tables 3, 4) are in good agreement with the results of other investigations [1, 15], and our

Table 2 Chemical composition (wt%) of χ-phase and σ-phase after isothermal aging

Element	σ-phase	χ-phase
Mo	7.5 ± 0.8	13.0 ± 0.9
Cr	26.7 ± 1.1	24.0 ± 0.7
Ni	1.4 ± 0.1	3.6 ± 0.1

Table 3 Mo, Cr, and Ni content (wt%) of χ-phase after solution annealing and continuous cooling treatment

Cooling rate (°C/s)	Solution annealing at 1020 °C			Solution annealing at 1050 °C		
	Mo	Cr	Ni	Mo	Cr	Ni
0.03	14.3	25.2	2.7	15.2	26.0	2.9
0.05	11.8	25.2	2.9	16.1	25.7	3.0
0.10	11.2	24.3	3.3	12.0	26.1	3.5

Table 4 Mo, Cr, and Ni content (wt%) of σ-phase after solution annealing and continuous cooling treatments

Cooling rate (°C/s)	Solution annealing at 1020 °C			Solution annealing at 1050 °C		
	Mo	Cr	Ni	Mo	Cr	Ni
0.03	8.4	28.5	3.1	7.8	28.7	2.9
0.05	7.3	27.2	3.3	8.0	28.8	3.0
0.10	7.3	27.3	3.0	7.5	25.9	3.5
0.20	7.3	27.3	3.0	7.3	27.5	3.2
0.25	6.1	25.5	3.7	8.3	26.6	3.3
0.30	6.1	25.1	4.0	6.8	27.0	3.5
0.35	5.6	25.4	3.9	7.0	26.1	3.8

results on σ-phase composition are near the values of equilibrium σ-phase composition [1].

The χ-phase composition is characterized by a significant higher content of molybdenum, nearly twice the Mo content of the σ-phase. Therefore, it is quite easy to distinguish these two phases through SEM-BSE imaging.

After isothermal aging, with our treatment conditions, the chemical composition of both χ-phase and σ-phase seems not be related to time, temperature and phase amount, in agreement with [20]. However, the possible variation of σ-phase composition with aging time and temperature have been verified in some other DSS [21] and also after very long time, 6 months, aging treatments in 2205 and 2507 grades [22].

On the contrary, the composition of the secondary phases in the continuous cooled samples is significantly related to the solution annealing temperature and mainly to the cooling rates (Tables 3, 4). As the cooling rate decreases, in both σ and χ-phases the molybdenum and chromium contents gradually increase, approaching the values obtained in the isothermal tests.

The most significant variation concerns the molybdenum content. In the σ-phase, Mo content varies from 4.6%, at the highest cooling rate, to 8%, at the lowest cooling rate. Given that the base alloy contains about 3% Mo, the large composition variation can be justified considering that the σ-phase and χ-phase formation is strongly dependent on diffusion. At the highest cooling rates, there is not sufficient time for diffusion to supply adequate molybdenum (and chromium) amounts to reach the equilibrium composition. Therefore, the highest cooling rates produce σ-phase and χ-phase at the lowest alloying elements content.

In addition, the formation of the χ-phase is even more affected by the restriction of the time for diffusion, owing to its highest molybdenum content.

The χ-phase precipitation is associated with the longest allowed diffusion times: the isothermal aging and the lowest cooling rates. This could be justified because the χ-phase nucleation is favored by smaller coherency strains than σ-phase in the ferrite lattice [2]. On the contrary, the χ-phase formation needs a more effective diffusion, because of the higher molybdenum content. Therefore, in experimental conditions with the longest diffusion time, i.e., isothermal aging tests and continuous cooling at low rates, nucleation prevails and the χ-phase appears as the first precipitating phase.

Results on the composition variations of σ and χ phase in the 2507 steel are similar to that observed in the 2205.

These results seem to indicate the conditioning affect of diffusion on the precipitation sequence and moreover that the role of the χ-phase, as the stable σ-phase precursor in the DSS, is not a general phenomenon, but depends on the steel composition (mainly on the molybdenum content) and can occur only with specific conditions of solution annealing temperature or cooling rates. This, perhaps, could also justify some discrepancies between various results previously reported [11, 12, 23–25], concerning the sequence of secondary phases formation in DDS.

2304 and 2101 DSS

The first effect of the aging treatments is the increase in the austenite content, which is more relevant in the 2304 steel at 750 and 850 °C, than in the 2101 steel. At 750 °C, for example, the amount of austenite in 2304 increased to 53.1% after 45 min of aging and to 54.6% after 90 min of aging. The increase in the austenite content is due to the formation of secondary austenite.

However, in both steels, the aging treatments did not produce the precipitation of χ or σ-phases, as usually occurs in more conventional 2205 and 2507, nickel

alloyed, DSS, even for very long soaking times, over 750 h [5, 13]. Instead in the 2101 steel the precipitation of small black particles (in the SEM-BSE images) at the ferrite/ferrite and ferrite/austenite grain boundaries was observed. In Fig. 6a, a schematic of the precipitation kinetics and an example of a BSE micrograph (Fig. 6b: 700 °C, 150 h aging) are shown. The precipitates were analyzed by EDS (close to the resolution limit), and an evident enrichment of chromium was observed. By referring to other different experimental observations reported in the literature, such small black particles can be identified as chromium nitrides, although it cannot be excluded that some of them are chromium carbides.

In the 2304 steel, no precipitation of black particles was observed after aging at 550 and 650 °C, but a precipitation of same black particles was observed after 40–45 min of aging at 750 and 850 °C. The precipitation of the nitrides, in this steel, therefore, requires higher temperatures and longer times.

In this grade, the precipitates are close to the austenite/ferrite grain boundaries and seldom inside the austenitic grains. This precipitation occurs jointly with the formation of secondary austenite [5] (named also $\gamma 3$, while $\gamma 2$ is the austenite coming directly from the ferrite transformation). This is confirmed by the results of the image analysis that indicate an increase in the austenite content during the aging at 750 and 850 °C. Moreover, the EDS analysis shows that the concentration of Cr in the ferrite and austenite phases is around 28 and 22 wt%, respectively, while its concentration in this secondary austenite $\gamma 3$ is 19.2 wt%. In the secondary austenite $\gamma 3$, Cr depletion is thus observed, because of the formation of the precipitates. In addition, the concentration of Ni is 3.2 and 6.5 wt% in ferrite and austenite phases, respectively, and 5 wt% in this secondary austenite. This means that the Cr-depleted regions, formerly ferritic, and transformed to secondary austenite $\gamma 3$ as a consequence of nitrides formation, are enriched by the Ni that diffuse into it from the surrounding already austenitic regions. Therefore, the formation of secondary austenite $\gamma 3$ seems to involve both the depletion of Cr and the enrichment of Ni of these transformed regions.

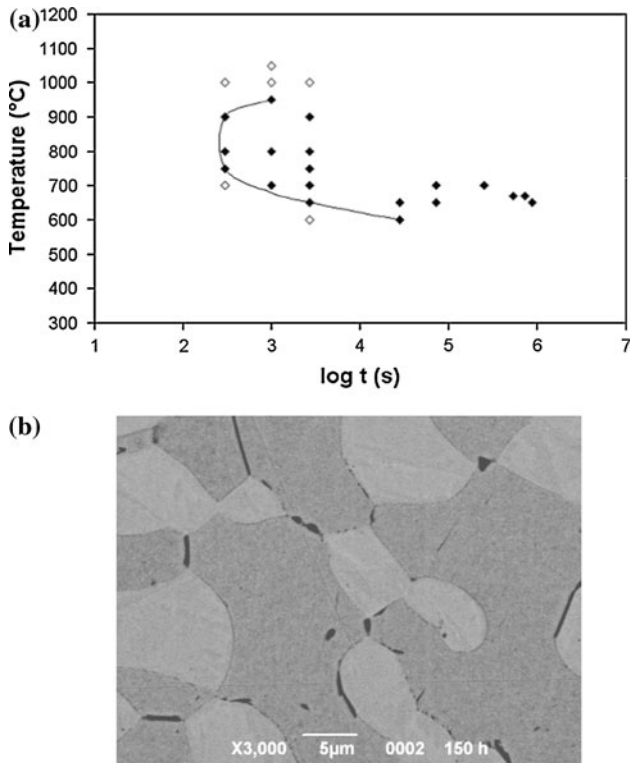

Fig. 6 Nitrides precipitation in 2101 DSS: **a** kinetics schematic, **b** 700 °C, 150 h (BSE image)

The very low Ni content in the 2101 grade could explain why in this grade the secondary austenite $\gamma 2$ formation appear less important, in agreement with Thermocalc indications. In this grade the nitrides remain almost always located at the grain boundaries (Fig. 6b).

Ni-alloyed (2205 and 2507) versus Mn-alloyed (2101 and 2304) DSS

As regards the phases transformations in Ni-alloyed and Mn-alloyed DSS during isothermal aging, the difference more evident is the lack of σ precipitation in the latter, despite the Thermocalc calculations forecast the presence of σ phase between the stable constituents in all the four DSS considered. The temperature ranges of σ stability arrive at low temperatures as 400 °C, and still lower for Ni-alloyed DSS. However, in all the grades, and particularly in the Ni-alloyed DSS, the σ-phase precipitation at temperatures below 650 °C cannot be observed, or can occur only after extremely long soaking times, over 1000 h. These results emphasize how decreasing the temperature, also the diffusion and precipitation rate in all the considered DSS grades decrease.

The previous experimental results indicate that during isothermal aging the intermetallic phases can form in a rather short times in the Ni-alloyed DSS (in the temperature range 850–950 °C, see "Isothermal aging" section for more details), but, on the contrary, in the Mn-alloyed DSS the precipitation is very sluggish and a significant presence of such phases cannot be detected also after very long time aging treatments. This behavior clearly arises from the difference in the precipitation kinetic from the metastable solid solutions obtained in the four steels, by quenching from the high temperatures of the solution annealing treatment. The formation of the same intermetallic phases is rather rapid in the Ni-alloyed DSS and much slower in the Mn-alloyed DSS.

The different precipitation kinetics can be justified by various effects. First of all, in the Thermocalc diagrams is evident that the temperature range of formation and stability of intermetallic phases is lower, below 800 °C, in the Mn-alloyed DSS, than in the Ni-alloyed DSS, below 1000 °C. Obviously, by decreasing the precipitation temperature the diffusion and precipitation rate decrease.

Moreover, the Thermocalc diagrams highlight the TCP phase formation in Ni-alloyed DSS occurring in the same temperature range, 700–1000 °C, of the transformation of the ferrite to secondary austenite giving a strong decrease of the ferrite content which in the 2205 grade fully disappears in the 800–900 °C temperature range. This allows the development of the transformation of ferrite in austenite and TCP phases ($\alpha \rightarrow \gamma 3 + \sigma + \chi$) following the favorable mechanism of the eutectoid transformation, so reducing the diffusion path necessary for the alloy elements redistribution in the new phases.

On the contrary, the equilibrium behavior of the Mn-DSS is very different in several aspects: first in these grades, the χ-phase formation is not forecast by Thermocalc, moreover, the σ-phase temperature formation is clearly lower, below 800 °C, and finally this temperature is also lower than the temperature of secondary austenite $\gamma 2$ formation, which also in these grades occur in the 800-1000 °C range, as in the Ni-DSS.

Moreover, in the Mn-DSS such secondary austenite formation is quantitatively less important and the ferrite content is never below 30%. All these peculiarities can strongly affect the formation kinetics of the σ-phase, which become sluggish both because occurring at lower temperatures, and because cannot be supported by the favorable mechanism of the eutectoid transformations, occurring as ferrite transformation to both σ and secondary austenite.

As a further effect, the differences in composition have to be considered. In the Mn-DSS both Ni and Mo contents are much lower than in the Ni-DSS. The low Mo content reduces, or avoids, the possible formation of the χ-phase, the first and more rapid precipitating phase, active also as precursor of the σ-phase during isothermal treatments. But the low Mo content should make more difficult also the σ-phase formation, as suggested by [26], in agreement with our experimental results, despite the indications of Thermocalc equilibrium diagrams. Finally the lower Ni content increases the ferrite stability and reduces the possible formation of secondary austenite not allowing the eutectoid formation of austenite and TCP phases.

The concluding remark of our results could be that while in the Ni-alloyed DSS the TCP phase precipitation is clearly related to the secondary austenite formation, this is not the same in the Mn-alloyed DSS. A further confirmation could be derived from the analysis of the behavior of another grade, similar to the 2101, but having some minor,

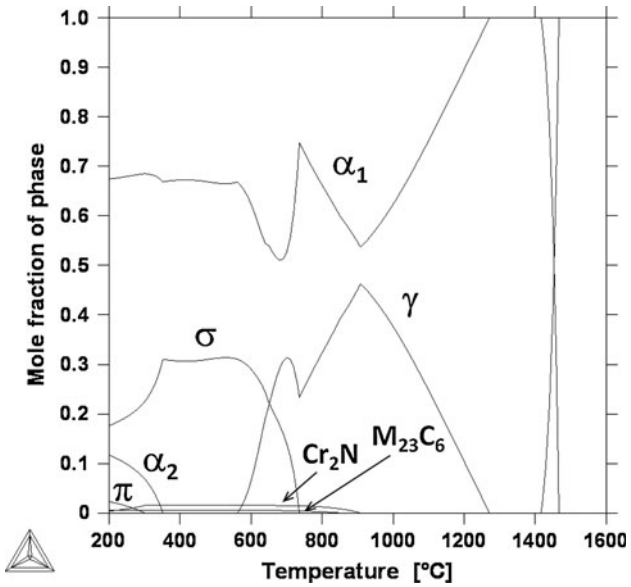

Fig. 7 Phase diagram of 2101 with modified composition

but significant differences in composition from the grade in Table 1: Mn 3.95 and N 0.13% that is a lower content of austenite stabilizer components. Also in this new grade, the TCP phases precipitation was completely absent, as in the previous grade, despite the obviously different pattern of austenite/ferrite phases stability, as shown in the corresponding Thermocalc diagram in Fig. 7. The differences in composition induce an evident decrease of secondary austenite formation, but this do not seems to have any influence on the stability, temperature range, etc., of the TCP formation, which seems to be independent on ferrite/austenite transformation and stability in the Mn-alloyed DSS examined.

Finally, it should be considered that Thermocalc calculations indicate the equilibrium phases which should be present in the alloys at different temperatures. As concerning our experimental results, obviously the microstructures obtained after CCT are non-equilibrium microstructures; therefore, they can be different from Thermocalc indications.

However, also the results of our isothermal aging tests are the microstructures deriving from a particular solid state transformation and the decomposition of the metastable solid solution coming from the solution annealing treatment. Obviously, the resulting microstructures are strongly affected by diffusion phenomena and kinetic peculiarities of the solid state formation of the new (equilibrium) phases. Therefore, our results indicate that kinetic of the precipitation of the sigma (equilibrium) phase from the oversaturated metastable solid solution is rapid in the Ni–Mo alloyed (2205 and 2507) DSS but not in the Mn-alloyed (2101 and 2304) DSS, where also long time aging

treatments, about 1000 h, are not sufficient for the equilibrium microstructure formation.

Conclusions

Results of the analysis of the TCP phase's formation in the four DSS examined can be summarized:

- Equilibrium data indicate the possible formation of TCP phases in all the DSS considered, in the range between from 1000–750 to 400 °C.
- In the Ni-Mo alloyed DSS, both χ and σ-phases precipitation occurs, according equilibrium data: in isothermal tests the χ is the first precipitating phase but in the CCT this phase appears only at lower cooling rates than the σ-phase.
- In the Mn-alloyed DSS, the formation of σ-phase cannot be detected also after long time isothermal aging; as equilibrium phases, only the nitrides formation have been revealed.
- The different behavior of TCP formation in the four DSS could be justified by differences in kinetic and mechanism of precipitation of the new TCP phase from the metastable solid solutions obtained from the solution annealing.

References

1. Nilsson JO (1992) Mater Sci Technol 8:685
2. Nilsson JO, Huhtala T, Karlsson L (1996) Metall Mat Trans 27A:2196
3. Charles J (2008) Steel Res Int 79:445
4. Lo KH, Lai JKL, Shek CH, Li DJ (2007) Mater Sci Eng A 452:78
5. Johansson P, Liljas M (2001) Avesta Polarit Corros Manag Appl Eng 24:24
6. Calliari I, Ramous E, Zanesco M (2006) J Mater Sci 41:7643. doi: 10.1007/s10853-006-0857-2
7. Karlsson K (1997) In: Proceedings of 5th World Conference, Duplex Stainless Steel 97, vol 73. KCI, Zutphen
8. He YL, Zhu NQ, Lu XG, Li L (2010) Mater Sci Eng A 528:721
9. Calliari I, Pellizzari M, Ramous E (2011) Mater Sci Technol 27:928
10. Calliari I, Zanesco M, Ramous E, Bassani P (2007) JMEPEG 16: 109
11. Chen TH, Wenig KL, Yang JR (2002) Mater Sci Eng A 338:259
12. Chen TH, Yang JR (2001) Mater Sci Eng A 311:28
13. Calliari I, Brunelli K, Zanellato M, Ramous E, Bertelli R (2009) J Mater Sci 44:3764. doi:10.1007/s10853-009-3505-9
14. Kim SB, Paik KW, Kim YG (1998) Mater Sci Eng A 247:67
15. Johnson E, Kim YJ, Scott Chumbley L, Gleeson B (2004) Scr Mater 50:1351
16. Calliari I, Brunelli K, Dabalà M, Ramous E (2003) JOM 61:80
17. Kaufman L, Bernstein H (1970) In: Computer calculation of phase diagram, Man. Labs. Inc. Cambdridge, Mass/Academic Press, New York
18. Sundman B, Jansson B, Anderson JO (1985) CALPHAD 9:153
19. Pohl M, Storz O, Glogoski T (2007) Mater Charact 58:65
20. Dobranszky J, Szabo PJ, Berecz T, Hrotko V, Portko M (2004) Spectrochim Acta B 59:1781
21. Lo KH, Sheck Ch, Zhang WW, Wong KW (2010) J Mater Sci 45:1790. doi:10.1007/s10853-009-4156-6
22. Wessman S, Petterson R, Hertzman (2010) Steel Res Int 82:337
23. Toor JU, Hyun PJ, Kwon HS (2008) Corr Sci 50:404
24. Lee KM, Cho HS, Choi DC (1999) J Alloys Compd 285:156
25. Ahn YS, Kang JP (2000) Mater Sci Technol 16:382
26. Sieurin H, Sandstrom R (2007) Mater Sci Eng A 444:271